Testing a linear relation: short-range correlations and the EMC effect for gluons and quarks in nuclei*

Shu-Man Hu (胡书曼)[1] Wei Wang (王伟)[2†] Ji Xu (徐吉)[1‡] Xing-Hua Yang (杨兴华)[3§] Shuai Zhao (赵帅)[4¶]

[1]Frontiers Science Center for Rare Isotopes, and School of Nuclear Science and Technology, Lanzhou University, Lanzhou 730000, China
[2]INPAC, Key Laboratory for Particle Astrophysics and Cosmology (MOE), Shanghai Key Laboratory for Particle Physics and Cosmology, School of Physics and Astronomy, Shanghai Jiao Tong University, Shanghai 200240, China
[3]School of Physics and Optoelectronic Engineering, Shandong University of Technology, Zibo, Shandong 255000, China
[4]Department of Physics, School of Science, Tianjin University, Tianjin 300350, China

Abstract: In this work, we focus on the possible linear relationship between short-range correlations (SRCs) and the EMC effect for partons in nuclei. First, we test a linear relationship pertaining to gluons in bound nuclei; it is manifested as a correlation between the slope of the reduced cross-section ratio in deep inelastic scattering (DIS) and the cross-section of sub-threshold J/ψ photoproduction. For comparison, results from four different global analysis groups of nuclear parton distribution functions (nPDFs) are utilized. These results show a good linear correlation between the gluons in bound nuclei and the slope of the reduced cross-section ratio, consistent with the possible presence of nuclear effects in the gluon distributions. Second, we investigate the linear relationship of quarks in the proton-induced Drell-Yan process. The corresponding results for quarks show strong sensitivity to the parameterizations forms adopted by the different groups. These findings enhance our understanding of the substructure in bound nuclei and provide a valuable reference for future global fitting of nPDFs.

Keywords: short-range correlations, nuclear parton distribution functions, EMC effect

DOI: 10.1088/1674-1137/ae62f8 **CSTR:** 32044.14.ChinesePhysicsC.50073106

I. INTRODUCTION

The nuclei consist of strongly interacting protons and neutrons, which give rise to the vast majority of mass in the visible universe. Inclusive lepton scattering is an effective tool for studying nuclei. Previously, it was widely believed that the quark structure within nucleons would not be influenced by the structure of atomic nuclei due to energy scale separation. However, the European Muon Collaboration discovered that the per-nucleon deep inelastic scattering (DIS) cross-section of iron to deuteron is degressive at $0.3 \leqslant x \leqslant 0.7$, which is now known as the EMC effect [1]. Since then, the EMC effect has been confirmed in different nuclei [2−7], indicating that the quark structure is significantly modified by the nuclear medium. The origin of the EMC effect has numerous explanations [8−13], yet a consensus remains elusive. Recent studies considering the relation between the EMC effect and nucleon-nucleon short-range correlations (SRCs) have attracted a lot of attention [14−19]. The SRC is a strongly interacting nucleon pair with a large relative momentum and a small center-of-mass momentum in comparison to the single-nucleon Fermi momentum, and this short-range interaction may cause a modification of the structure of the nucleon.

The authors in Ref. [14] quantified the relationship between these two effects through a linear correlation between the SRC scaling factor and the size of the EMC effect. In line with this idea, a similar linear correlation was proposed between the heavy flavor production in DIS and sub-threshold photoproduction of J/ψ, which are two gluon-centric processes [20]. It is noteworthy that, while some studies regard SRCs as a key transitional structure connecting quark-gluon and nucleonic degrees of freedom [21], others contend that current experimental data are also compatible with non-SRC interpretive

Received 25 January 2026; Accepted 15 April 2026; Accepted manuscript online 16 April 2026
* Supported in part by the National Natural Science Foundation of China (12125503, 12335003, 12105247, 12305106, 12475098)
† E-mail: wei.wang@sjtu.edu.cn
‡ E-mail: xuji@lzu.edu.cn
§ E-mail: yangxinghua@sdut.edu.cn
¶ E-mail: zhaos@tju.edu.cn

frameworks [22].

Therefore, a better understanding of the nuclear parton (quark and gluon) distributions and SRCs requires more careful examination [23−28]. The linear relation presented in Ref. [20] relies on the global analysis of gluon nuclear parton distribution functions (nPDFs) in EPPS21 [29]. When extracting the nPDFs, different collaboration groups may adopt different experimental data and parameterizations forms. Would this linear relationship still hold across different groups? Currently, a feasible approach is to collect and compare all available fitting results for gluon nPDFs in the market. In this work, we present a detailed analysis of this issue by employing four commonly used nPDF parameterizations: EPPS21[1] [29], nNNPDF3.0(no LHCb D)[2] [30], nCTEQ15HQ[3] [31], and TUJU21[4] [32]. Furthermore, most of these datasets are also incorporated in the LHAPDF library [33].

The study of the EMC effect through the proton-induced Drell-Yan process holds unique importance as a complementary probe to DIS. By selecting kinematic regions sensitive to quark distributions of the nuclear target, these experiments can test the specific suppression of quarks in bound nucleons (EMC effect) [34−38]. In this work, we also investigate the linear relationship of quarks in the proton-induced Drell-Yan process by utilizing the nPDFs of these four groups.

This paper is organized as follows. In Sec. II, the linear relation of gluons proposed in DIS and sub-threshold photoproduction of J/ψ processes are tested. In Sec. III, we examine the linear relation of quarks in the proton-induced Drell-Yan process. Sec. IV is reserved for conclusions. Some additional tables and figures are collected in the appendices.

II. TEST OF LINEAR RELATION OF GLUONS

Exploring gluon EMC effects requires the knowledge of the nPDFs pertaining to gluons. The construction of an electron-ion collider (EIC) with the possibility to operate with a wide variety of nuclei will constrain the gluon density in nuclei via measurements of the charm reduced cross section in DIS [39].

$$\sigma^{c\bar{c}}_{A,\mathrm{red}}(x,Q^2) \equiv \left(\frac{\mathrm{d}\sigma^{c\bar{c}}_{A}}{\mathrm{d}x\mathrm{d}Q^2}\right)\frac{xQ^4}{2\pi\alpha^2[1+(1-y)^2]} = \frac{2}{[1+(1-y)^2]}\left(xy^2F^{c\bar{c}}_{1,A}(x,Q^2)+(1-y)F^{c\bar{c}}_{2,A}(x,Q^2)\right). \quad (1)$$

Here, $\sigma^{c\bar{c}}_{A}$ denotes the charm cross section, which is customarily expressed as the reduced cross section $\sigma^{c\bar{c}}_{A,\mathrm{red}}$; x and y are the Bjorken variable and inelasticity, respectively. In the parton model, information about the gluon nPDFs is encoded in the $F^{c\bar{c}}_{1/2,A}$, which are called charm structure functions.

$$F^{c\bar{c}}_{1,A}(x,Q^2) = \int_{\tau x}^{1}\frac{\mathrm{d}z}{z}f^{A}_{g}(z,\hat{s})\,f_1\left(\frac{x}{z},Q^2\right),$$
$$F^{c\bar{c}}_{2,A}(x,Q^2) = \int_{\tau x}^{1}\frac{\mathrm{d}z}{z}z f^{A}_{g}(z,\hat{s})\,f_2\left(\frac{x}{z},Q^2\right). \quad (2)$$

Here, f^{A}_{g} is the gluon nPDF in a given nucleus A; $f_{1/2}$ represents the perturbative partonic cross sections, whose expressions can be found in [40].

Next, we define a ratio factor $R^{c\bar{c}}_{A}$ to quantitatively assess the nuclear modification in different nuclei.

$$R^{c\bar{c}}_{A}\left(x,Q^2\right) = \frac{\sigma^{c\bar{c}}_{A,\mathrm{red}}\left(x,Q^2\right)}{A\sigma^{c\bar{c}}_{N,\mathrm{red}}\left(x,Q^2\right)}, \quad (3)$$

where $\sigma^{c\bar{c}}_{N,\mathrm{red}}\left(x,Q^2\right)$ in the denominator denotes the reduced cross section in an electron-proton (considered free) collision. By utilizing the global analyses of the EPPS21, nNNPDF3.0 (no LHCb D data), TUJU21, and nCTEQ15HQ collaborations, we can present this ratio factor $R^{c\bar{c}}_{A}$ as a function of x for nuclei including ^{3}He, ^{4}He, ^{9}Be, ^{12}C, ^{27}Al, ^{56}Fe, ^{131}Xe, and ^{197}Au, as illustrated in Fig. 1. Here, with $Q^2 = 10\,\mathrm{GeV}^2$ and $\sqrt{s} = 20\,\mathrm{GeV}$, we are considering the kinematics expected at the forthcoming EIC [41]. It is noteworthy that the EPPS21 analysis uses the CT18ANLO set as its free proton baseline [42], whereas the other three analyses provide free proton PDFs determined within their own respective global analysis frameworks.

It can be observed that the results from all four groups exhibit "EMC-like" behavior in terms of gluons. While the shapes vary, this ratio factor $R^{c\bar{c}}_{A}$ consistently decreases for different nuclei in the intermediate x-region. In the nCTEQ15HQ results, the behaviors of light nuclei and heavy nuclei are distinctly different. For light nuclei, this ratio steadily increases. This significant discrepancy shown in nCTEQ15HQ compared to other groups indicates our incomplete understanding of gluon nPDFs and suggests a need for reassessment of the parameterizations in nCTEQ15HQ.

The magnitude of the gluon EMC effect for nucleus A can be quantified by fitting the slope of the reduced cross-section ratio $R^{c\bar{c}}_{A}$, *i.e.*, $(-\mathrm{d}R^{c\bar{c}}_{A}/\mathrm{d}x)$. Based on Fig. 1,

1) https://research.hip.fi/qcdtheory/nuclear-pdfs/epps21/
2) https://nnpdf.mi.infn.it/for-users/nnnpdf3-0/
3) https://ncteq.hepforge.org/ncteq15hq/index.html
4) https://lhapdf.hepforge.org/pdfsets.html

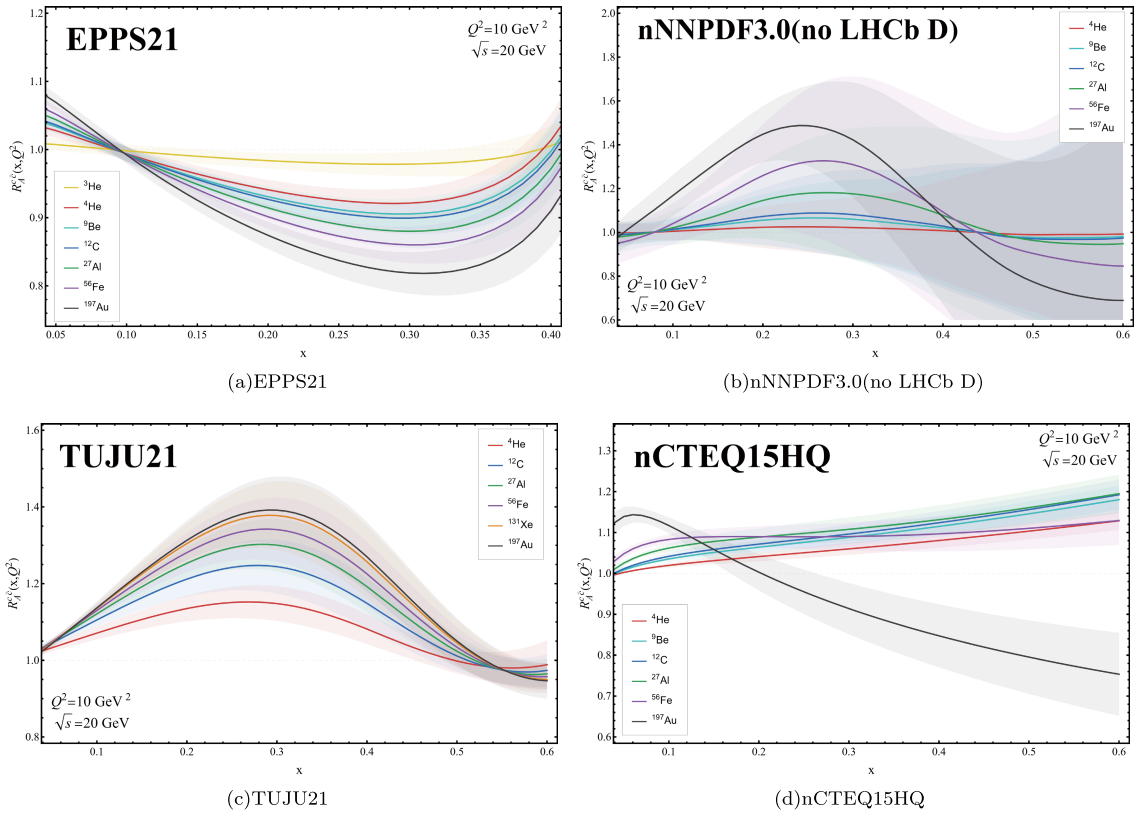

Fig. 1. (color online) $R_A^{c\bar{c}}\left(x,Q^2\right)$ is defined in Eq. (3) as a function of x using the results of global analyses from different groups. The typical kinematics chosen are $Q^2=10\,\mathrm{GeV}^2$, $\sqrt{s}=20\,\mathrm{GeV}$. The solid lines in different colors represent different nuclei, and the corresponding bands represent the uncertainties in the nPDFs given by different groups, as indicated by the legends.

the fitting range within the "EMC-like" region can be determined, which is chosen as $0.1\leqslant x\leqslant 0.2$ for EPPS21, and $0.3\leqslant x\leqslant 0.4$ for nNNPDF3.0 (no LHCb D), nCTEQ15HQ, and TUJU21. We further expand the fitting range by 50% for each, serving as a source of systematic uncertainty in our analysis. The obtained results are collected in Tables A1−A4 in Appendix A.

The authors in Ref. [20] applied the chiral effective field theory (χEFT) and proposed a linear relation between the slope of reduced cross-section ratios and the J/ψ photoproduction cross-section at the photon energy $E_\gamma=7.0\,\mathrm{GeV}$ in the nucleus rest frame.

$$-\frac{\mathrm{d}R_A^{c\bar{c}}(x,Q^2)}{\mathrm{d}x}=C'(x,Q^2)(\sigma_A^{\mathrm{sub}}/A)\big|_{E_\gamma\sim 7\,\mathrm{GeV}}\,. \tag{4}$$

Here, the function $C'(x,Q^2)$ does not depend on the type of nucleus A. In addition, the ratio of cross sections is linked to the ratio of gluon nPDFs by the following formula [20].

$$\frac{\sigma_A^{\mathrm{sub}}/A}{\sigma_{A'}^{\mathrm{sub}}/A'}\bigg|_{E_\gamma\sim 7\,\mathrm{GeV}}\simeq\frac{\left(f_g^A(x,Q^2)/f_g^N(x,Q^2)\right)-1}{\left(f_g^{A'}(x,Q^2)/f_g^N(x,Q^2)\right)-1}\,, \tag{5}$$

where $f_g^N(x,Q^2)$ is the gluon PDF in a free nucleon. It has been argued that this ratio is independent of x and Q^2, indicating these dependencies cancel out on the right-hand side of Eq. (5). Here, we corroborate this characteristic by presenting three-dimensional visualizations of this ratio. The nucleus A' in the denominator is chosen to be ^{12}C. One can observe that in all the subplots in Fig. 2, this ratio displays a plateau with small variations. The value of the ratio can be determined by fitting the heights of these plateaus. Currently, there is very little experimental data available for the sub-threshold production of J/ψ. We therefore use the calculated per-nucleon cross section in γ^{12}C collision $(\sigma_{\mathrm{C}}^{\mathrm{sub}}/12)=14.37\,\mathrm{pb}$ at the photon energy $E_\gamma\sim 7\,\mathrm{GeV}$ in a recent theoretical work [20]. Therefore, the per-nucleon cross section for different nuclei can be extrapolated. The quantitative outcomes are presented in Tables A1−A4 in Appendix A.

Analyzing the information delineated in these tables, we plot the gluon EMC slopes versus the cross sections for sub-threshold J/ψ production in Fig. 3. One can find that a linear correlation exists between $(-\mathrm{d}R_A^{c\bar{c}}/\mathrm{d}x)$ and $(\sigma_A^{\mathrm{sub}}/A)$. Specifically, we have

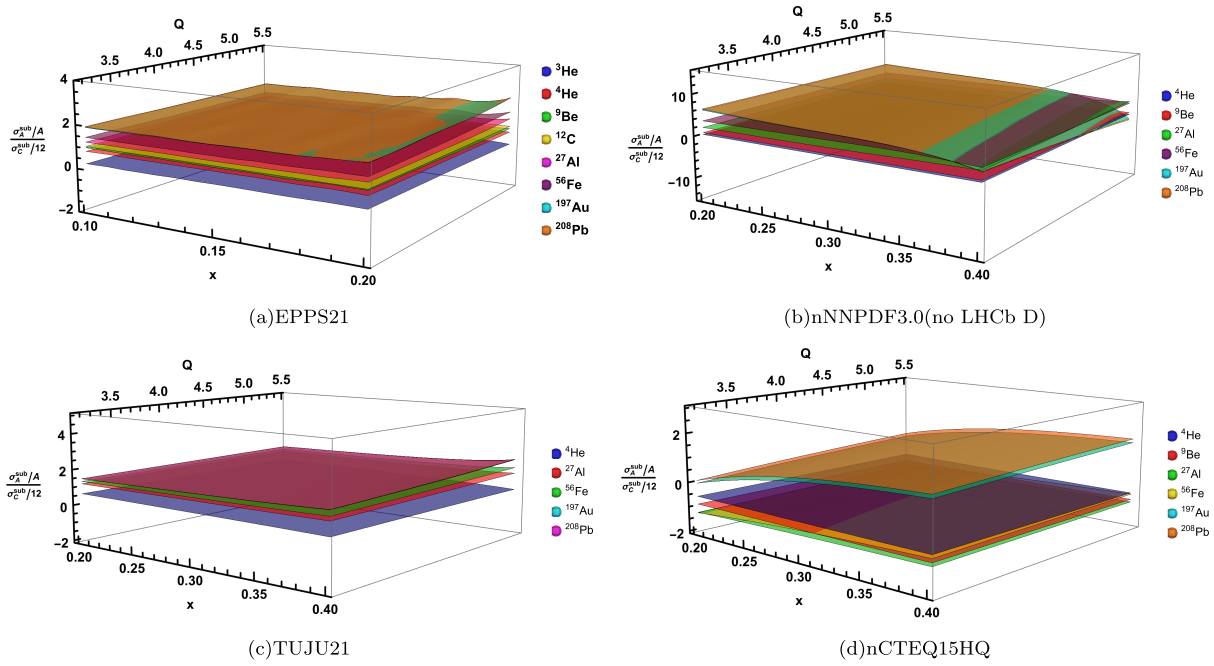

(a)EPPS21 (b)nNNPDF3.0(no LHCb D)

(c)TUJU21 (d)nCTEQ15HQ

Fig. 2. (color online) The ratio $\frac{\sigma_A^{\rm sub}/A}{\sigma_{A'}^{\rm sub}/A'}$ in Eq. (5) for different nuclei with respect to Carbon, at different values of x and Q^2.

EPPS21 :

$$-{\rm d}R_A^{c\bar{c}}/{\rm d}x = (0.044 \pm 0.002) \times (\sigma_A^{\rm sub}/A) - (0.008 \mp 0.014), \tag{6a}$$

nNNPDF3.0(noLHCbD) :

$$-{\rm d}R_A^{c\bar{c}}/{\rm d}x = (0.043 \pm 0.002) \times (\sigma_A^{\rm sub}/A) - (0.029 \mp 0.019), \tag{6b}$$

TUJU21 :

$$-{\rm d}R_A^{c\bar{c}}/{\rm d}x = (0.054 \pm 0.009) \times (\sigma_A^{\rm sub}/A) + (0.262 \pm 0.111), \tag{6c}$$

nCTEQ15HQ :

$$-{\rm d}R_A^{c\bar{c}}/{\rm d}x = (0.025 \pm 0.005) \times (\sigma_A^{\rm sub}/A) + (0.058 \pm 0.062). \tag{6d}$$

Although the fitted slopes and intercepts differ significantly, the results of the three groups EPPS21, nNNPDF3.0 (no LHCb D), and TUJU21 all exhibit an apparent linear relationship. The linear relationship presented by nCTEQ15HQ is less clear, but it broadly aligns with Eq. (4). In nCTEQ15HQ, the steadily increasing behavior of $R_A^{c\bar{c}}\left(x, Q^2\right)$ for light nuclei in Fig. 1(d) results in negative sub-threshold cross sections, which are not physically meaningful. However, the compliance with the linear relation in Eq. (4) shown in Fig. 3(d) is still noteworthy. On the other hand, the negative cross sections stress the need for a reassessment of the parameterizations in nCTEQ15HQ.

The χEFT provides us with a method for scale separation, which naturally leads to the linear relation in Eq. (6). What we want to highlight is that the scale separation itself provides valuable information, such as the existence of a linear relationship, regardless of the specific slope and intercept values. The results obtained here support the conclusions in Ref. [20], but also underscore our limited knowledge of gluon nPDFs, whose errors are not taken into account. However, the introduction of the ratio factor $R_A^{c\bar{c}}$ would help to reduce the corresponding uncertainties substantially. Furthermore, the isoscalar correction dependencies of nPDFs are significantly less pronounced in gluons compared to quarks. At the end of this section, we wish to emphasize that Fig. 3 serves as an indication, not a demonstration. Therefore, future experimental validation (or negation) of this linear relationship is imperative.

III. TEST OF LINEAR RELATION OF QUARKS

Apart from DIS, Drell-Yan production of lepton pairs from nucleons is another important tool for studying the quark structure of nucleons [43−45], which inherently involves the antiquark distributions of either the beam or target hadron. The EMC effect has been experimentally studied in Drell-Yan reactions [46−49]. In proton-induced Drell-Yan, a quark (antiquark) with momentum

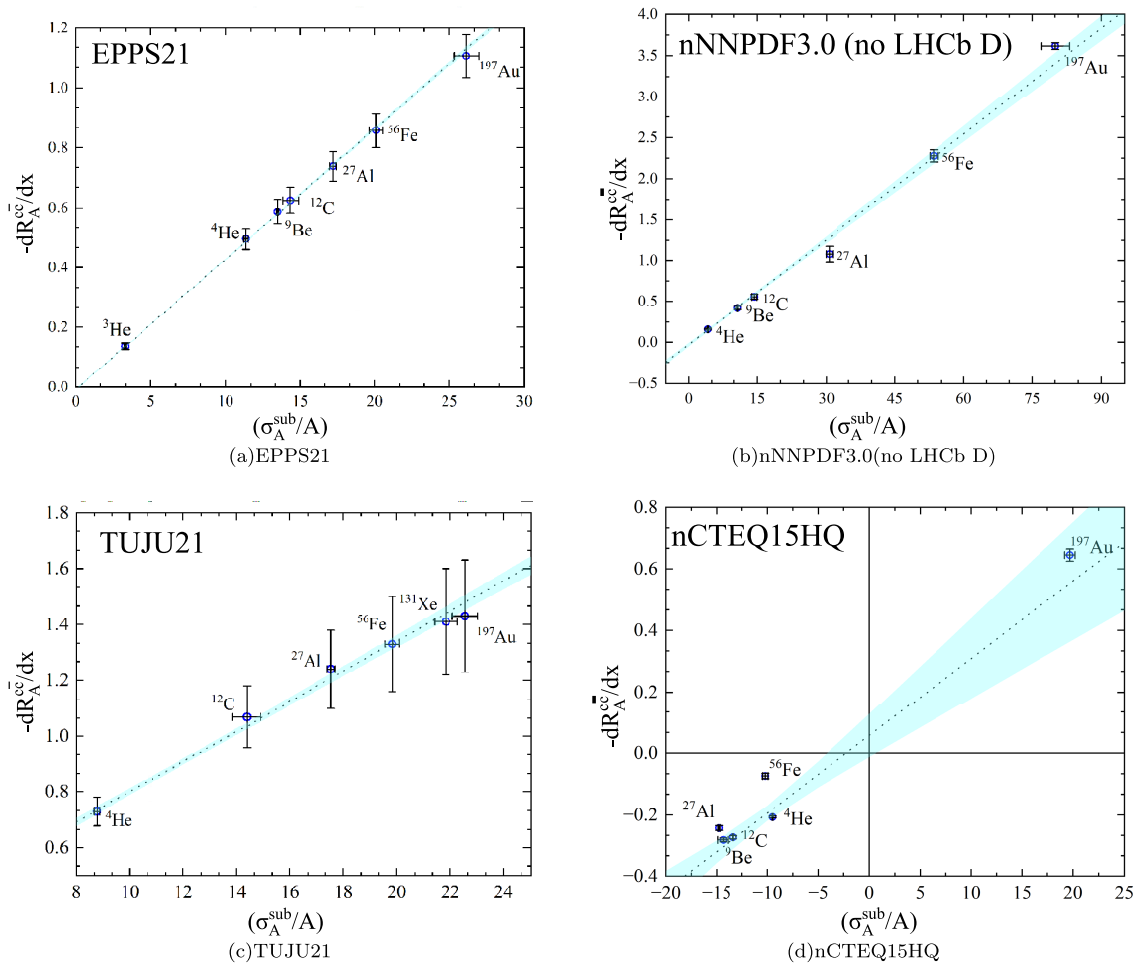

Fig. 3. (color online) The linear relation between the slope of nuclear modification $(-dR_A^{c\bar{c}}/dx)$ and the sub-threshold cross section (σ_A^{sub}/A) is investigated. The gluon nPDFs are adopted from different collaborations (EPPS21, nNNPDF3.0 (no LHCb D), TUJU21, and nCTEQ15HQ, respectively). The black dashed lines correspond to fits of numerical results, and the shaded bands represent the 1σ standard deviation derived from the linear fit to the values of these data points.

fraction x_1 from the beam proton and an antiquark (quark) of the target nucleon with momentum fraction x_2 annihilate via a virtual photon into a charged-lepton pair. This process is illustrated in Fig. 4.

The corresponding cross-section depends on the charge-squared-weighted sum of quark and antiquark distributions in the beam and the target nucleon [50–51].

$$\frac{d^2\sigma_{DY}(pA)}{dx_1dx_2} = K\frac{4\pi\alpha^2}{9Q^2}\sum_q e_q^2\left[f_q^p(x_1,Q^2)f_{\bar{q}}^A(x_2,Q^2) + f_{\bar{q}}^p(x_1,Q^2)f_q^A(x_2,Q^2)\right]. \quad (7)$$

The invariant mass of the lepton pair, denoted by Q, is given by $Q^2 = sx_1x_2$. The summation is taken over quark flavors; α is the fine-structure constant; e_q is the charge of a quark or antiquark of flavor q; and $f_{q(\bar{q})}^{p(A)}$ corresponds to the quark (antiquark) PDF in the proton (nucleus). The factor K absorbs higher-order QCD corrections, which is approximately $K \sim 1+(\alpha_s/2\pi)(4\pi^2/3)+O(\alpha_s^2)$ [52].

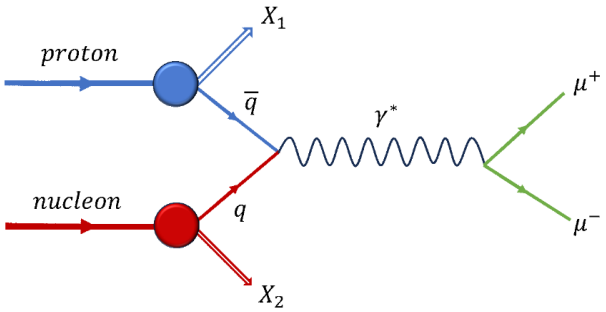

Fig. 4. (color online) The proton-induced Drell-Yan process at leading order.

In Eq. (7), the nuclear dependence comes from the modification of (anti)quark distributions in the target nucleus. The quark distributions of nucleus A are constructed as

$$f_q^A(x,Q^2)=\frac{Zf_q^{p/A}(x,Q^2)+(A-Z)f_q^{n/A}(x,Q^2)}{A}. \tag{8}$$

With Z being the atomic charge number, here $f_q^{p(n)/A}$ represents the quark PDF of a proton (neutron) bound in the nucleus A. Since we are interested in the EMC effect of the nucleon, we integrate the variable x_1 and formally obtain:

$$\frac{\mathrm{d}\sigma_{\mathrm{DY}}(pA)}{\mathrm{d}x_2}=K\frac{4\pi\alpha^2}{9Q^2}\sum_q e_q^2\left[f_{\bar{q}}^A(x_2,Q^2)\int_0^1\mathrm{d}x_1 f_q^p(x_1,Q^2)+f_q^A(x_2,Q^2)\int_0^1\mathrm{d}x_1 f_{\bar{q}}^p(x_1,Q^2)\right]. \tag{9}$$

Thus, a ratio factor can be defined to quantify the nuclear modification in different nuclei relative to deuterons:

$$R_A^{\mathrm{DY}}\left(x_2,Q^2\right)=\frac{\mathrm{d}\sigma_{\mathrm{DY}}(pA)/\mathrm{d}x_2}{\mathrm{d}\sigma_{\mathrm{DY}}(pD)/\mathrm{d}x_2}. \tag{10}$$

We can depict this R_A^{DY} by utilizing nPDFs from EPPS21, nNNPDF3.0 (no LHCb D), TUJU21, and nCTEQ15HQ. Figure 5 shows a comparison of these results with the data from the Fermilab E772 experiment for a number of nuclear targets [47, 49]. In the existing experimental data, it is difficult for x_2 to surpass 0.4, since the absolute cross section would become very small. We set $Q^2=25\,\mathrm{GeV}^2$ and $\sqrt{s}=40\,\mathrm{GeV}$, consistent with the kinematics of typical Drell-Yan experiments such as E772 and E866 [34, 47]. The kinematic constraint $x_1x_2=Q^2/s$ yields a lower integration limit for $x_{1,\min}\approx 0.0156$ with $x_{2,\max}=1$. Thus, the numerical integration is performed over $x_1\in[0.0156, 1]$. From Fig. 5, it can be observed that the shapes of the ratio R_A^{DY} for EPPS21, nCTEQ15HQ, and TUJU21 are closely aligned, while nNNPDF3.0 (no LHCb D) shows a marked deviation from the others. These results show that the predictions of R_A^{DY} are sensitive to the nPDF sets used as input in the calculations.

It is important to emphasize that the proton-induced Drell-Yan process involves the quark and antiquark distributions of both the beam proton and the target nucleon. Given our focus on the nucleon's substructure, we attribute the two terms in Eq. (9) to contributions from the nucleon's antiquark and quark distributions, respectively. We present these two contributions:

$$\begin{cases}\sum_q e_q^2\left[f_{\bar{q}}^A(x_2,Q^2)\int_{x_{1,\min}}^1\mathrm{d}x_1 f_q^p(x_1,Q^2)\right],\\ \sum_q e_q^2\left[f_q^A(x_2,Q^2)\int_{x_{1,\min}}^1\mathrm{d}x_1 f_{\bar{q}}^p(x_1,Q^2)\right],\end{cases} \tag{11}$$

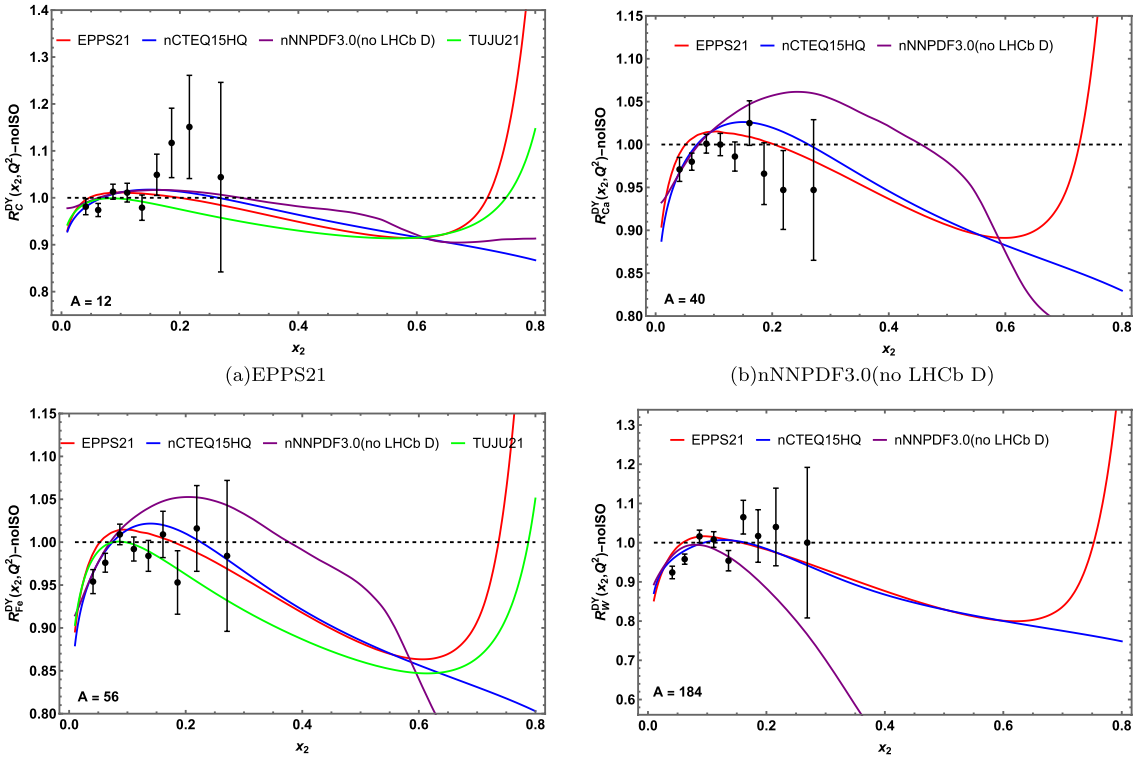

(a)EPPS21 (b)nNNPDF3.0(no LHCb D)

(c)TUJU21 (d)nCTEQ15HQ

Fig. 5. (color online) The ratio of proton-induced Drell-Yan differential cross sections as a function of x_2 in different nuclei, with typical kinematics chosen as $Q^2=25\,\mathrm{GeV}^2$ and $\sqrt{s}=40\,\mathrm{GeV}$.

and compare their magnitudes in Fig. 6. Within the EMC region of interest, the contribution from the target nucleon's quark distributions is predominant. Notably, for the nNNPDF3.0 (no LHCb D) case, the nucleon's quark contribution becomes smaller than the antiquark's when $x_2 \gtrsim 0.7$, a behavior that diverges from other global analyses. As noted in Ref. [30], this arises because experimental constraints on large-x_2 nuclear antiquarks are limited, causing the methodological assumptions in the fit to play a more significant role. By restricting x_2 to the interval $x_2 \in [0.2, 0.6]$, the contribution from the nucleon's antiquark distributions can be safely removed.

$$\frac{\mathrm{d}\sigma_{\mathrm{DY}}(pA)}{\mathrm{d}x_2} = K\frac{4\pi\alpha^2}{9Q^2} \times \left[\sum_q e_q^2\left(f_q^A(x_2,Q^2)\int_{x_{1,\min}}^1 \mathrm{d}x_1 f_{\bar{q}}^p(x_1,Q^2)\right)\right]. \tag{12}$$

The observation of EMC effects in the medium-x_2 region is plausible. The magnitude of the EMC effect in different nuclei can be quantified by fitting the slope of R_A^{DY}, just as we did for $R_A^{c\bar{c}}$ in the previous section.

To account for the unequal number of protons and neutrons in certain nuclei, one can include an isoscalar correction factor (ISO), which is defined as [6].

$$\mathrm{ISO} = \frac{\frac{A}{2}\left(1+\frac{\sigma_n}{\sigma_p}\right)}{Z+N\frac{\sigma_n}{\sigma_p}}. \tag{13}$$

where σ_n and σ_p are the elementary electron-neutron and electron-proton cross sections, respectively. The calculation of their ratio σ_n/σ_p is model-dependent; here, we adopt $\sigma_n/\sigma_p = 1 - 0.8x_2$ [7]. This correction factor adjusts the per-nucleon cross section for nucleus A to a new value that represents the per-nucleon cross section for a "virtual nucleus" A with equal numbers of neutrons and protons. We present in Fig. 7 the ratio R_A^{DY} computed using the ISO factor for four different nPDF sets. The results from EPPS21 and TUJU21 are generally consistent with each other, whereas those from nCTEQ15HQ, and especially nNNPDF3.0 (no LHCb D), show distinct behaviors.

The results for the slopes of R_A^{DY} in the EMC region are collected in Tables B1−B4 in Appendix B. The fitting range is $0.35 \leqslant x_2 \leqslant 0.45$ for the nPDFs of EPPS21, nCTEQ15HQ, and TUJU21. For nNNPDF3.0 (no LHCb D), the fitting range is $0.25 \leqslant x_2 \leqslant 0.35$. We further expanded the range by 50% for each, serving as a source of systematic uncertainty in our analysis. We combine these results with the SRC scaling factor $a_2(A)$ measured in lepton inelastic scattering (collected in Tables B1−B4 in

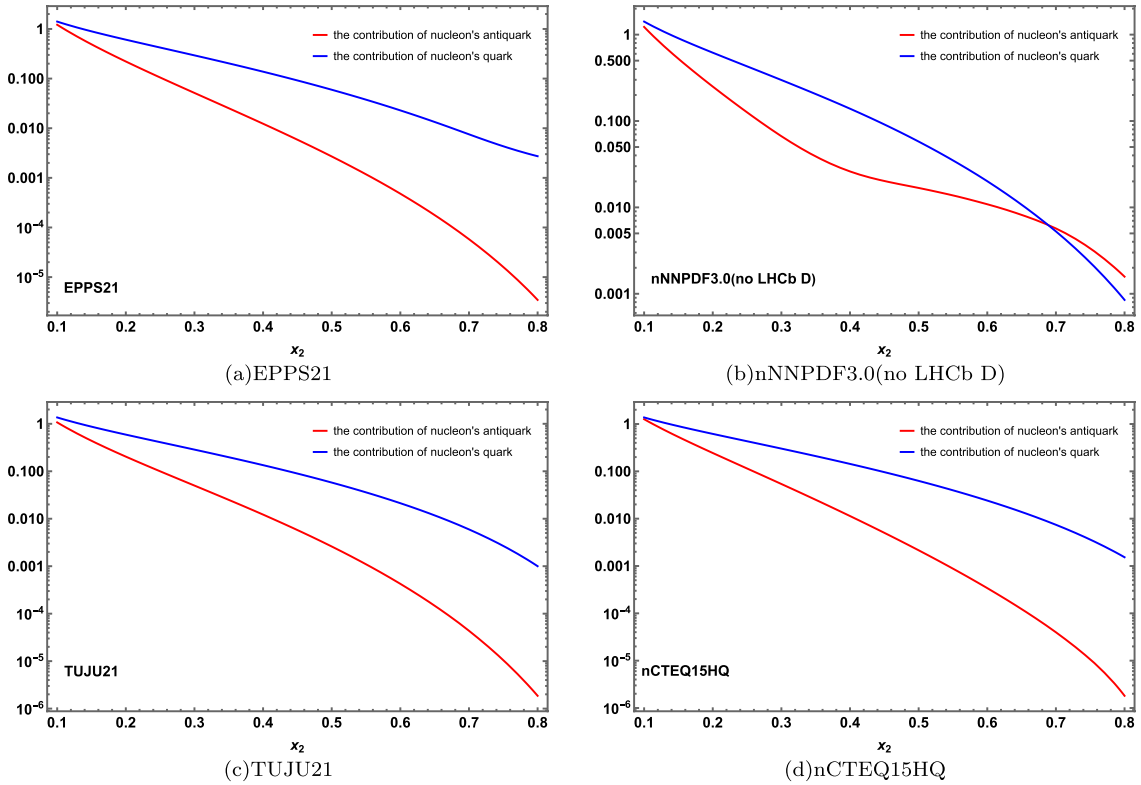

(a)EPPS21 (b)nNNPDF3.0(no LHCb D)

(c)TUJU21 (d)nCTEQ15HQ

Fig. 6. (color online) Comparison between the contributions from the antiquark and quark distributions of the target nucleon (^{56}Fe) in Eq. (7). The typical kinematics are chosen as $Q^2 = 25\,\mathrm{GeV}^2$.

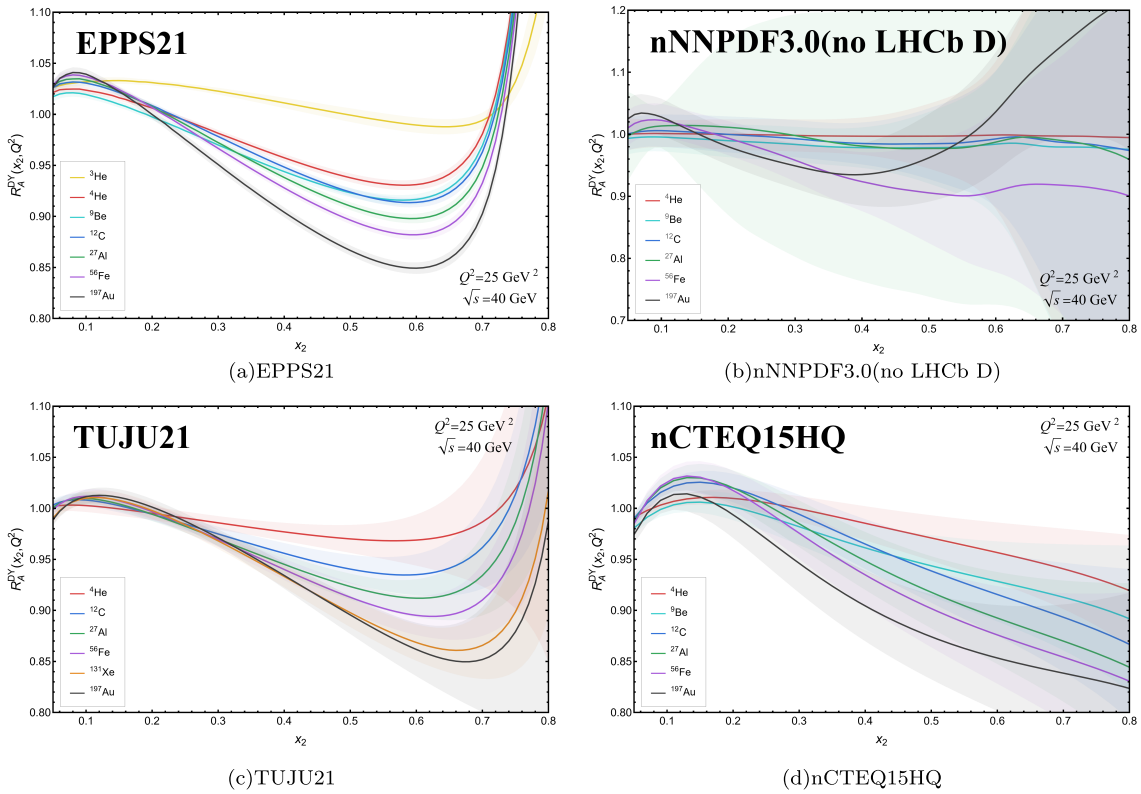

(a)EPPS21 (b)nNNPDF3.0(no LHCb D)

(c)TUJU21 (d)nCTEQ15HQ

Fig. 7. (color online) $R_A^{\rm DY}\left(x_2,Q^2\right)$ is defined in Eq. (10) as a function of x_2 using the global analyses from different groups. The typical kinematics are chosen as $Q^2=25\,{\rm GeV}^2$ and $\sqrt{s}=40\,{\rm GeV}$. The solid lines in different colors represent different nuclei, and the corresponding bands represent the uncertainties in the nPDFs given by different groups, as indicated by the legends.

Appendix B) [6], which approximately equals the relative abundance of SRC pairs in a nucleus compared to deuteron. Figure 8 shows the slopes versus the SRC scaling factors. The black line corresponds to a fit of the numerical results.

EPPS21 :

$$-{\rm d}R_A^{\rm DY}/{\rm d}x_2=(0.092\pm0.005)\Big(a_2(A)-a_2(D)\Big), \qquad (14a)$$

nNNPDF3.0(noLHCbD) :

$$-{\rm d}R_A^{\rm DY}/{\rm d}x_2=(0.048\pm0.013)\Big(a_2(A)-a_2(D)\Big), \qquad (14b)$$

TUJU21 :

$$-{\rm d}R_A^{\rm DY}/{\rm d}x_2=(0.065\pm0.012)\Big(a_2(A)-a_2(D)\Big), \qquad (14c)$$

nCTEQ15HQ :

$$-{\rm d}R_A^{\rm DY}/{\rm d}x_2=(0.074\pm0.006)\Big(a_2(A)-a_2(D)\Big). \qquad (14d)$$

Here we constrain the fit by forcing the slope to go through zero for the deuteron ($a_2(D)=1$) [53]. It can be observed in Fig. 8 that the result of EPPS21 exhibits the strongest linear relationship, followed by nCTEQ15HQ and TUJU21, with nNNPDF3.0(no LHCb D) being the least favorable. The EPPS21 and nCTEQ15HQ include constraints from Drell-Yan data in their fits, which likely helps capture the nuclear modification of valence quarks in the medium-x region relevant to the EMC effect. However, the TUJU21 analysis does not include Drell-Yan data, which may explain why its quark-level linearity is less pronounced. The nNNPDF3.0(no LHCb D) employs a Monte Carlo approach with neural-network parameterizations (256 free parameters), which minimizes model bias but lacks strong constraints on medium to large-x nuclear antiquarks, propagating into the slope extraction and potentially weakening the linear correlation with SRC scaling factors. In addition, it can be observed from Fig. 7 that the uncertainties of quark nPDFs from the nNNPDF3.0(no LHCb D) are considerably larger than those from the other groups. Consequently, the reliability of the results derived from this group is diminished.

The universality of the linear relation across parton species is a natural prediction of SRC-driven nuclear modification models, where the local nuclear environ-

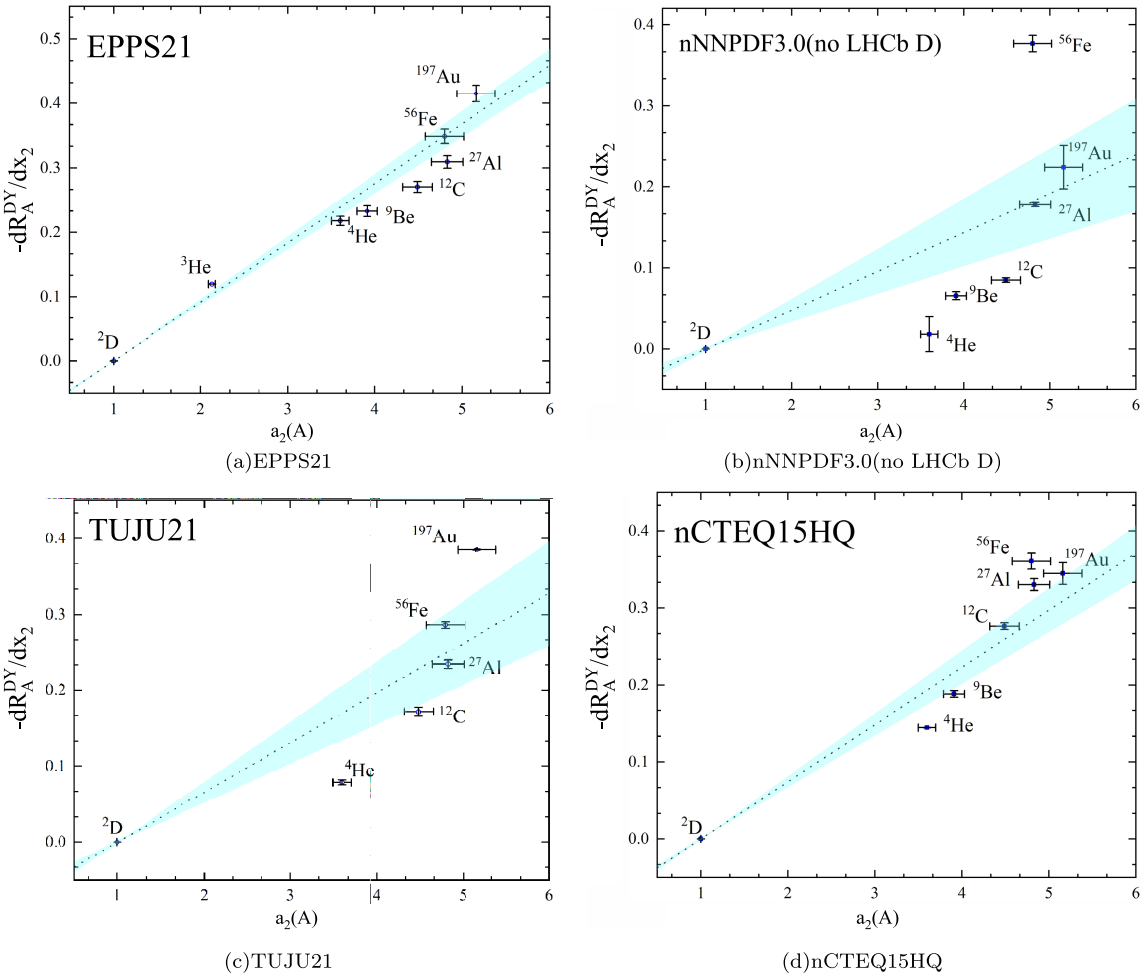

(a)EPPS21 (b)nNNPDF3.0(no LHCb D)

(c)TUJU21 (d)nCTEQ15HQ

Fig. 8. (color online) The linear relation between the slope of $R_A^{\rm DY}(x_2, Q^2)$ and the SRC scaling factor $a_2(A)$ is examined. The quark nPDFs are adopted from different groups (EPPS21, nNNPDF3.0 (no LHCb D), TUJU21, and nCTEQ15HQ, respectively). The black dashed lines correspond to fits of numerical results, which are normalized to a reference point with $-{\rm d}R_A^{\rm DY}(D)/{\rm d}x_2 = 0$ and $a_2(D) = 1$. The shaded bands correspond to the 1σ standard deviation derived from the linear fit to the values of these data points.

ment (*i.e.*, the presence of high-momentum nucleon pairs) alters the quark and gluon distributions in a correlated way. Therefore, in our opinion, the results that fail to reproduce this linear relationship warrant careful re-examination, particularly since the quark-related linearity has been well-established in DIS experiments. Given this prior knowledge, its manifestation in the proton-induced Drell-Yan process is also expected. It is worth stressing that the linear relationships exhibited by EPPS21 and nCTEQ15HQ in Fig. 8 are remarkably similar to the experimentally established relationship from DIS data [6], both with and without ISO corrections, as detailed in Fig. C1 in Appendix C. This observation is not intended to invalidate the results from the other groups. Rather, it underscores a pronounced tension in the current literature: the discrepancies between the predictions of different groups, as seen in Fig. 8, are substantial and merit further investigation. Future experimental data over a larger region of x_2 ($0.4 \leqslant x_2 \leqslant 0.7$) will help clarify this issue.

IV. SUMMARY

The EMC effect, which refers to the modification of quark distributions in bound nucleons compared to free ones, has been extensively studied over the past forty years. However, a comprehensive understanding of it is still lacking. How does the nuclear environment play an important role even at energy scales much higher than those involved in typical nuclear ground-state processes? Although the data do not yet allow for a clear preference between various explanations, the SRC-driven EMC effect offers a natural way forward. It is the local nuclear structure (SRCs) rather than the global nuclear environment that affects the distributions of partons, and this change is "averaged" in the per-nucleon cross section ratio in DIS experiments.

This study extends the previous work presented in Ref. [20]. First, focusing on gluons, we utilize four different nPDF parameterizations from EPPS21, nNNPDF3.0

(no LHCb D), nCTEQ15HQ, and TUJU21 to test the linear relation between the slope of the reduced cross section ratio in DIS and the cross section of sub-threshold photoproduction on J/ψ. Additionally, we investigate the linear relationship of quarks in the proton-induced Drell-Yan process with these four parameterizations. Our results show that the linear relation between the EMC effect and SRCs is consistently supported for gluons across all four nPDF sets, although the detailed slope and intercept values differ. For quarks, however, the validity of the linear relation exhibits a strong dependence on the nPDF parameterizations: EPPS21 and nCTEQ15HQ show good agreement with the SRC-scaling hypothesis, while nNNPDF3.0(no LHCb D) deviates significantly. The results of TUJU21 fall in between. These findings provide a useful reference for future global fits of nPDFs and highlight the need for improved constraints on quark nPDFs in the medium-x region.

APPENDIX A: COLLECTION OF $-\mathrm{d}R_A^{c\bar{c}}/\mathrm{d}x$ AND $(\sigma_A^{\mathrm{sub}}/A)$

Here, we collect the slopes of the ratio factor $-\mathrm{d}R_A^{c\bar{c}}/\mathrm{d}x$ and the per-nucleon cross sections for sub-threshold J/ψ photoproduction $(\sigma_A^{\mathrm{sub}}/A)$ to test the linear relation of gluons. The values are calculated using four different global analyses of nPDFs.

Table A1. The values of the slopes $-\mathrm{d}R_A^{c\bar{c}}/\mathrm{d}x$ and the per-nucleon cross sections $(\sigma_A^{\mathrm{sub}}/A)$ are calculated using the global analysis from EPPS21.

Nucleus	$-\mathrm{d}R_A^{c\bar{c}}/\mathrm{d}x$	$\sigma_A^{\mathrm{sub}}/A$
^{3}He	0.135 ± 0.010	3.31 ± 0.06
^{4}He	0.495 ± 0.035	11.35 ± 0.14
^{9}Be	0.587 ± 0.040	13.49 ± 0.07
^{12}C	0.624 ± 0.042	14.37 ± 0.54
^{27}Al	0.738 ± 0.049	17.23 ± 0.23
^{56}Fe	0.857 ± 0.056	20.09 ± 0.42
^{197}Au	1.106 ± 0.073	26.13 ± 0.82

Table A2. Same as Table A1, except using the global analysis from nNNPDF3.0 (no LHCb D).

Nucleus	$-\mathrm{d}R_A^{c\bar{c}}/\mathrm{d}x$	$\sigma_A^{\mathrm{sub}}/A$
^{4}He	0.155 ± 0.011	4.17 ± 0.14
^{9}Be	0.415 ± 0.019	10.78 ± 0.09
^{12}C	0.558 ± 0.029	14.37 ± 0.54
^{27}Al	1.079 ± 0.097	30.61 ± 0.68
^{56}Fe	2.279 ± 0.073	53.46 ± 0.80
^{197}Au	3.618 ± 0.041	80.04 ± 3.10

Table A3. Same as Table A1, except using the global analysis from TUJU21.

Nucleus	$-\mathrm{d}R_A^{c\bar{c}}/\mathrm{d}x$	$\sigma_A^{\mathrm{sub}}/A$
^{4}He	0.730 ± 0.054	8.77 ± 0.12
^{12}C	1.070 ± 0.109	14.37 ± 0.54
^{27}Al	1.240 ± 0.135	17.53 ± 0.14
^{56}Fe	1.330 ± 0.169	19.83 ± 0.27
^{131}Xe	1.408 ± 0.190	21.84 ± 0.42
^{197}Au	1.432 ± 0.200	22.56 ± 0.48

Table A4. Same as Table A1, except that the global analysis from nCTEQ15HQ is used.

Nucleus	$-\mathrm{d}R_A^{c\bar{c}}/\mathrm{d}x$	$\sigma_A^{\mathrm{sub}}/A$
^{4}He	-0.207 ± 0.003	-9.48 ± 0.04
^{9}Be	-0.273 ± 0.006	-13.36 ± 0.02
^{12}C	-0.282 ± 0.006	-14.37 ± 0.54
^{27}Al	-0.243 ± 0.008	-14.80 ± 0.10
^{56}Fe	-0.074 ± 0.009	-10.20 ± 0.26
^{197}Au	0.645 ± 0.020	19.69 ± 0.50

APPENDIX B: COLLECTION OF $-\mathrm{d}R_A^{\mathrm{DY}}/\mathrm{d}x_2$ AND $a_2(A)$

Here, we collect the slopes of the ratio factor

Table B1. The slopes of the ratio $-\mathrm{d}R_A^{\mathrm{DY}}/\mathrm{d}x_2$ and the SRC scaling factor $a_2(A)$ are calculated using the global analysis from EPPS21.

Nucleus	$-\mathrm{d}R_A^{\mathrm{DY}}/\mathrm{d}x_2$	$a_2(A)$
^{3}He	$0.12\pm9\times10^{-5}$	2.13 ± 0.04
^{4}He	0.218 ± 0.007	3.60 ± 0.01
^{9}Be	0.233 ± 0.008	3.91 ± 0.12
^{12}C	0.271 ± 0.009	4.49 ± 0.17
^{27}Al	0.310 ± 0.010	4.83 ± 0.18
^{56}Fe	0.349 ± 0.011	4.80 ± 0.22
^{197}Au	0.416 ± 0.014	5.16 ± 0.22

Table B2. Same as Table B1, except using the global analysis from nNNPDF3.0 (no LHCb D).

Nucleus	$-\mathrm{d}R_A^{\mathrm{DY}}/\mathrm{d}x_2$	$a_2(A)$
^{4}He	0.018 ± 0.022	3.60 ± 0.01
^{9}Be	0.066 ± 0.005	3.91 ± 0.12
^{12}C	0.085 ± 0.003	4.49 ± 0.17
^{27}Al	0.178 ± 0.002	4.83 ± 0.18
^{56}Fe	0.377 ± 0.01	4.80 ± 0.22
^{197}Au	0.224 ± 0.027	5.16 ± 0.22

Table B3. Same as Table B1, except using the global analysis from TUJU21.

Nucleus	$-\mathrm{d}R_A^{\mathrm{DY}}/\mathrm{d}x_2$	$a_2(A)$
^{4}He	0.079 ± 0.003	3.60 ± 0.01
^{12}C	0.172 ± 0.006	4.49 ± 0.17
^{27}Al	0.234 ± 0.005	4.83 ± 0.18
^{56}Fe	0.286 ± 0.004	4.80 ± 0.22
^{197}Au	$0.385 \pm 5.1 \times 10^{-4}$	5.16 ± 0.22

Table B4. Same as Table B1, except using the global analysis from nCTEQ15HQ.

Nucleus	$-\mathrm{d}R_A^{\mathrm{DY}}/\mathrm{d}x_2$	$a_2(A)$
^{4}He	$0.145 \pm 2.3 \times 10^{-4}$	3.60 ± 0.01
^{9}Be	0.188 ± 0.004	3.91 ± 0.12
^{12}C	0.276 ± 0.004	4.49 ± 0.17
^{27}Al	0.330 ± 0.008	4.83 ± 0.18
^{56}Fe	0.361 ± 0.010	4.80 ± 0.22
^{197}Au	0.345 ± 0.014	5.16 ± 0.22

$-\mathrm{d}R_A^{\mathrm{DY}}/\mathrm{d}x_2$ in the proton-induced Drell-Yan process and the SRC scaling factors $a_2(A)$ to test the linear relation of quarks. The values are calculated using four different global analyses of nPDFs.

APPENDIX C: COMPARISON OF LINEAR RELATION WITH AND WITHOUT ISO CORRECTIONS

To illustrate the effect of ISO corrections, Fig. C1

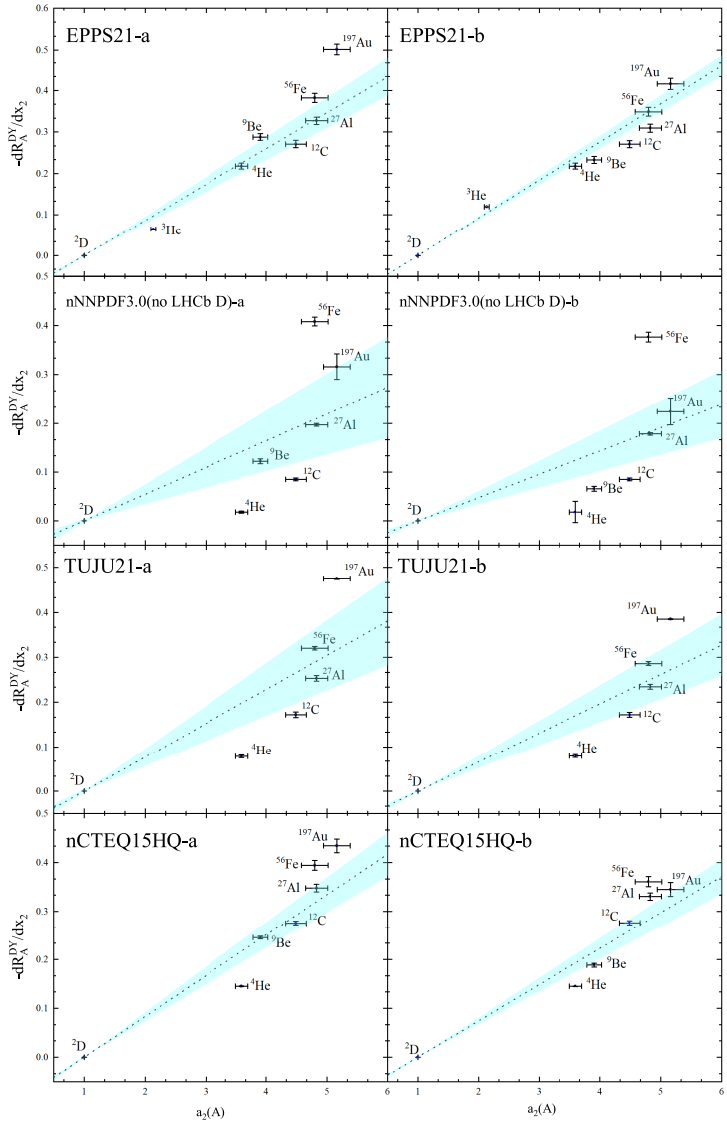

Fig. C1. A comparison of the linear relation for the four different groups with and without the ISO corrections is provided. The left panel shows the results without the ISO corrections (labeled "a"), while the right panel presents those with the ISO corrections applied (labeled "b").

shows the linear fitting results between the slopes of $R_A^{\rm DY}(x_2, Q^2)$ and the SRC scaling factors $a_2(A)$, both with and without ISO corrections. As observed, the $-{\rm d}R_A^{\rm DY}/{\rm d}x_2$ values show a noticeable reduction after applying the correction. This effect is more pronounced for nuclei with larger neutron-proton number differences.

References

[1] J. J. Aubert *et al*. (European Muon Collaboration), Phys. Lett. B **123**, 275 (1983)
[2] J. Ashman *et al*. (European Muon Collaboration), Phys. Lett. B **202**, 603 (1988)
[3] M. Arneodo *et al*. (European Muon Collaboration), Phys. Lett. B **211**, 493 (1988)
[4] D. Allasia *et al*. (New Muon (NMC) Collaboration), Phys. Lett. B **249**, 366 (1990)
[5] J. Seely, A. Daniel, D. Gaskell *et al*., Phys. Rev. Lett. **103**, 202301 (2009), arXiv: 0904.4448[nucl-ex]
[6] B. Schmookler *et al*. (CLAS Collaboration), Nature **566**(7744), 354 (2019), arXiv: 2004.12065[nucl-ex]
[7] J. Gomez, R. G. Arnold, P. E. Bosted *et al*., Phys. Rev. D **49**, 4348 (1994)
[8] R. Wang, N. N. Ma, and T. F. Wang, Chin. Phys. C **47**(4), 044103 (2023), arXiv: 2207.10980[nucl-th]
[9] G. F. Bertsch, L. Frankfurt, and M. Strikman, Science **259**, 773 (1993)
[10] G. A. Miller, Phys. Rev. C **89**(4), 045203 (2014), arXiv: 1311.4561[nucl-th]
[11] M. R. Frank, B. K. Jennings, and G. A. Miller, Phys. Rev. C **54**, 920 (1996), arXiv: nucl-th/9509030[nucl-th]
[12] R. Wang, X. Chen, and Q. Fu, Nucl. Phys. B **920**, 1 (2017), arXiv: 1611.03670[hep-ph]
[13] Y. Zhang, L. Shao, and B. Q. Ma, Nucl. Phys. A **828**, 390 (2009), arXiv: 0909.0454[nucl-th]
[14] L. B. Weinstein, E. Piasetzky, D. W. Higinbotham *et al*., Phys. Rev. Lett. **106**, 052301 (2011), arXiv: 1009.5666[hep-ph]
[15] O. Hen, M. Sargsian, L. B. Weinstein, E. Piasetzky *et al*., Science **346**, 614 (2014), arXiv: 1412.0138[nucl-ex]
[16] K. S. Egiyan *et al*. (CLAS Collaboration), Phys. Rev. Lett. **96**, 082501 (2006), arXiv: nucl-ex/0508026[nucl-ex]
[17] W. Wang, J. Xu, X. H. Yang *et al*., arXiv: 2409.14367 [hep-ph]
[18] O. Hen, E. Piasetzky, and L. B. Weinstein, Phys. Rev. C **85**, 047301 (2012), arXiv: 1202.3452[nucl-ex]
[19] M. Duer *et al*. (CLAS Collaboration), Nature **560**(7720), 617 (2018)
[20] W. Wang, J. Xu, X. H. Yang *et al*., Eur. Phys. J. A **61**(5), 112 (2025), arXiv: 2401.16662[hep-ph]
[21] A. W. Denniston *et al*. (nCTEQ Collaboration), Phys. Rev. Lett. **133**(15), 152502 (2024), arXiv: 2312.16293[hep-ph]
[22] P. Paakkinen, arXiv: 2510.00252 [hep-ph]
[23] J. Xu and F. Yuan, Phys. Lett. B **801**, 135187 (2020), arXiv: 1908.10413[hep-ph]
[24] Y. Hatta, M. Strikman, J. Xu *et al*., Phys. Lett. B **803**, 135321 (2020), arXiv: 1911.11706[hep-ph]
[25] J. W. Chen, W. Detmold, J. E. Lynn *et al*., Phys. Rev. Lett. **119**(26), 262502 (2017), arXiv: 1607.03065[hep-ph]
[26] X. G. Wang, A. W. Thomas, and W. Melnitchouk, Phys. Rev. Lett. **125**, 262002 (2020), arXiv: 2004.03789[hep-ph]
[27] X. H. Yang, F. Huang, and J. Xu, Phys. Rev. D **108**(5), 053005 (2023), arXiv: 2305.11538[hep-ph]
[28] F. Huang, J. Xu, and X. H. Yang, Phys. Rev. D **104**(3), 033002 (2021), arXiv: 2103.07873[hep-ph]
[29] K. J. Eskola, P. Paakkinen, H. Paukkunen *et al*., Eur. Phys. J. C **82**(5), 413 (2022), arXiv: 2112.12462[hep-ph]
[30] R. A. Khalek, R. Gauld, T. Giani *et al*., Eur. Phys. J. C **82**(6), 507 (2022), arXiv: 2201.12363[hep-ph]
[31] P. Duwentäster, T. Ježo, M. Klasen *et al*., Phys. Rev. D **105**(11), 114043 (2022), arXiv: 2204.09982[hep-ph]
[32] I. Helenius, M. Walt. and W. Vogelsang, Phys. Rev. D **105**(9), 094031 (2022), arXiv: 2112.11904[hep-ph]
[33] A. Buckley, J. Ferrando, S. Lloyd *et al*., Eur. Phys. J. C **75**, 132 (2015), arXiv: 1412.7420[hep-ph]
[34] M. A. Vasilev *et al*. (NuSea Collaboration), Phys. Rev. Lett. **83**, 2304 (1999), arXiv: hep-ex/9906010[hep-ex]
[35] P. E. Reimer (Fermilab SeaQuest Collaboration), EPJ Web Conf. **113**, 05012 (2016)
[36] P. E. Reimer (Fermilab SeaQuest Collaboration), J. Phys. Conf. Ser. **295**, 012011 (2011)
[37] P. Bordalo *et al*. (NA10 Collaboration), Phys. Lett. B **193**, 368 (1987)
[38] J. Badier *et al*. (NA3 Collaboration), Phys. Lett. B **104**, 335 (1981)
[39] E. C. Aschenauer, S. Fazio, M. A. C. Lamont *et al*., Phys. Rev. D **96**(11), 114005 (2017), arXiv: 1708.05654[nucl-ex]
[40] E. Laenen, S. Riemersma, J. Smith *et al*., Nucl. Phys. B **392**, 162 (1993)
[41] R. Abdul Khalek, A. Accardi, J. Adam *et al*., Nucl. Phys. A **1026**, 122447 (2022), arXiv: 2103.05419[physics.ins-det]
[42] T. J. Hou, K. Xie, J. Gao *et al*., arXiv: 1908.11394 [hep-ph]
[43] S. D. Drell and T. M. Yan, Phys. Rev. Lett. **25**, 316 (1970) [Erratum: Phys. Rev. Lett. **25**, 902 (1970)]
[44] F. Huang, S. M. Hu, D. M. Li *et al*., Eur. Phys. J. C **85**(10), 1225 (2025), arXiv: 2501.07059[hep-ph]
[45] T. Chmaj and K. J. Heller, Acta Phys. Polon. B **15**, 473 TPJU (1984)
[46] G. Moreno, C. N. Brown, W. E. Cooper *et al*., Phys. Rev. D **43**, 2815 (1991)
[47] D. M. Alde, H. W. Baer, T. A. Carey *et al*., Phys. Rev. Lett. **64**, 2479 (1990)
[48] J. G. Heinrich, C. E. Adolphsen, J. P. Alexander *et al*., Phys. Rev. Lett. **63**, 356 (1989)
[49] E866/E789/E772 web resources http://p25ext.lanl.gov/e866/papers/papers.html
[50] S. A. Kulagin and R. Petti, Phys. Rev. C **90**(4), 045204 (2014), arXiv: 1405.2529[hep-ph]
[51] I. R. Kenyon, Rept. Prog. Phys. **45**, 1261 (1982)
[52] G. Curci and M. Greco, Phys. Lett. B **92**, 175 (1980)
[53] J. Arrington, A. Daniel, D. Day *et al*., Phys. Rev. C **86**, 065204 (2012), arXiv: 1206.6343[nucl-ex]